Nanofluidic structures with complex three-dimensional surfaces

Nanofluidic structures with complex three-dimensional surfaces

Samuel M Stavis[1]**, Elizabeth A Strychalski**[2] **and Michael Gaitan**[1]

[1] Semiconductor Electronics Division, National Institute of Standards and Technology, Gaithersburg, MD 20899, USA
[2] Department of Physics, Cornell University, Ithaca, NY 14853, USA

E-mail: samuel.stavis@nist.gov, eas58@cornell.edu and michael.gaitan@nist.gov

Abstract

Nanofluidic devices have typically explored a design space of patterns limited by a single nanoscale structure depth. A method is presented here for fabricating nanofluidic structures with complex three-dimensional (3D) surfaces, utilizing a single layer of grayscale photolithography and standard integrated circuit manufacturing tools. This method is applied to construct nanofluidic devices with numerous (30) structure depths controlled from $\approx$10 to $\approx$620 nm with an average standard deviation of <10 nm over distances of >1 cm. A prototype 3D nanofluidic device is demonstrated that implements size exclusion of rigid nanoparticles and variable nanoscale confinement and deformation of biomolecules.

1. Introduction

In the last decade, attention has focused on the development of nanofluidic devices for the manipulation and analysis of biomolecules. Driven by the need for increased analytical ability in the life sciences, and the potential to elucidate nanometer scale and single molecule phenomena, lithographic microfabrication and nanofabrication processes developed by the semiconductor electronics industry have been adapted to construct fluidic devices with critical dimensions that enhance control over interactions with nanoscale analytes. When combined with sensitive optical and electronic metrology, nanofluidic devices have demonstrated unique advantages, which have motivated monolithic integration of these technologies with more complex analytical systems in accordance with the lab-on-a-chip concept [1, 2].

The utility of a nanofluidic device is often derived from the confinement, isolation and manipulation of analytes within engineered nanometer scale volumes. This approach has been used to control the conformation and behavior of a DNA molecule [3], for example, and to simultaneously improve its optical [4] or electronic [5] detection. Dimensions critical to this process include the chain diameter [6] or persistence length of a biopolymer [7], the wavelength of light [8], and the thickness of the electronic double layer [9]. Nanofluidic channels with various aspect ratios have figured prominently in these manipulations, including channels defined by two microscale (or larger) lateral dimensions and one nanoscale axial dimension. This type of axial nanostructure has been applied to physical studies of DNA conformation and dynamics [10], diffusion [11], and electrokinetic mobility [12], as well as applications including DNA barcoding [13] and separation by analyte motion across boundaries formed by arrays of constrictions within a channel [14].

To date, the vast majority of nanofluidic devices have been characterized by planar surfaces and simple features defined by one, two, or at most several device depths. As the functionality of a nanofluidic device is determined by its dimensionality and complexity [15], the development of more intricate three-dimensional structures would lead to enhanced control over nanometer scale fluidic environments and analytes, which could result in new or improved device utility. Progress in this regard has been limited by conventional nanofabrication processes [16], which are inherently planar and become increasingly restrictive when many layers of high resolution lithography are performed in a research facility. Two exceptions include diffraction gradient lithography [17] and nanoglassblowing [18]. Both are unconventional approaches to the fabrication and integration of non-planar nanofluidic devices with limited ability to pattern complex structures of arbitrary design. A variety of techniques have been developed for the fabrication of three-dimensional microfluidic [19] and submicrometer [20] fluidic structures with limited applicability to the fabrication of fluidic nanostructures.

Separately, in the last two decades, grayscale or graytone photolithography has been used to fabricate '3D' (denoting complex surface topography fabricated from the top-down) microstructures [21] and is a latent solution to the problem of fabricating 3D nanofluidic devices and other types of 3D axial nanostructures. Variations abound, but most grayscale techniques require only a single exposure of a photosensitive film to a pattern of spatially modulated intensity [22], which transcends the serial alignment and patterning of multiple device layers that limits planar nanofabrication processes. Grayscale photolithography has been used since its inception to fabricate 3D microstructures with curved and complex surfaces for diffractive optical elements [23] and more recently for microelectromechanical [24] and microfluidic devices [25]. The application of grayscale photolithography to the fabrication of nanofluidic devices has the potential to expand the scope of this technology by enabling the production of 3D nanostructures that would otherwise be impractical or impossible to make. Fluidic devices with three-dimensional surfaces defined by numerous depths or continuous contours spanning the nanometer length scale in the axial dimension would be able to perform more complex manipulations on a single nanoscale analyte or process a more complex mixture of nanoscale scale analytes than is feasible using conventional planar nanofluidic devices. These advantages could be exploited to improve the range or resolution of on-chip analytical applications and to conduct investigations of nanoscale or single molecule phenomena in unprecedented detail, as demonstrated here.

This paper presents the first 3D nanofluidic structures, fabricated using conventional integrated circuit manufacturing tools and a single layer of grayscale photolithography. As illustrated in figure 1, a chromium-on-quartz photomask of arbitrary design was used with a reduction stepper to pattern a 3D photoresist etch mask, and 30 nanoscale etch depths were transferred into a fused silica substrate with reactive ion etching to form complex three-dimensional surfaces. Glass wafer bonding was then used to form enclosed 3D nanofluidic structures. Nanoscale structure depths were controlled from ≈10 to ≈620 nm, with an average standard deviation for all structure depths of <10 nm over distances >1 cm, across several structures with staircase function surface topographies and different depth profiles and offsets. These designs were chosen to test and emphasize the limits of the nanofabrication process and as conceptually simple but structurally complex prototype 3D nanofluidic devices. As a demonstration of the potential utility of 3D nanofluidic devices, rigid nanoparticles and deformable biomolecules were manipulated in a nanofluidic channel with a staircase function depth profile ranging from ≈50 to ≈550 nm across the width of the structure. Polystyrene spheres were excluded from regions of the structure with depths less than the 100 nm sphere diameter, while λ DNA molecules assumed different conformations as a function of structure depth. These results suggest the future use of 3D nanofluidic devices for the high resolution spatial separation and metrology of complicated mixtures of nanoscale analytes, and the detailed study of nanoscale confinement effects on biopolymers and other nanoscale phenomena.

2. Grayscale optical theory

A chromium-on-quartz photomask is used in conjunction with a reduction stepper as a diffraction or spatial frequency filter [26–28], as illustrated in figure 1(A). The photomask is patterned with diffractive arrays of chromium squares of size s on a square lattice of pitch p. The reduction stepper illuminates the photomask with light of wavelength λ_s and partial coherence parameter σ_s, and the lithographic lens projects the device pattern onto the wafer with a reduction factor of $1/M_s$. With appropriate selection of s and p, diffractive orders other than zero are rejected by the lens aperture. As the zeroth diffractive order determines only the amplitude of the image intensity, individual elements within the diffractive arrays are not resolved, and a grayscale of uniform intensity results. The stepper resolution determines the critical aerial pitch [26]

$$p'_c = \frac{1}{1 + \sigma_s} \frac{\lambda_s}{\mathrm{NA}_s} \tag{1}$$

while the diagonal spacing between adjacent elements in the diffractive arrays on the photomask determines the critical square size [29]

$$s_c = p - \sqrt{\frac{p_c^2}{2}} \tag{2}$$

with $p_c = p'_c/M_s$. A prime denotes the aerial plane. Diffractive array pitches larger than p_c or squares smaller than s_c will result in fluctuations in aerial intensity as diffractive elements begin to resolve. When equations (1) and (2) are satisfied, the aerial image intensity of a grayscale is

$$I'_{\mathrm{GS}} = I_0 \left(1 - \left(\frac{s^2}{p^2} \right) \right)^2 \tag{3}$$

where I_0 is the incident illumination intensity.

3. Nanostructure fabrication

A staircase function grayscale aerial intensity pattern was rendered with diffractive arrays of chromium squares varying in size from $s = 1.37$ to 2.24 μm on a fixed pitch $p = 4.00$ μm. The photomask had a critical dimension tolerance of 15 nm (absolute error), critical dimension uniformity of 15 nm (maximum range) and an address unit of 5 nm, as specified by the manufacturer. Each of the 30 grayscales had an aerial width of 4.00 μm defined by diffractive arrays five square elements wide, as illustrated in figure 1(A). The aerial grayscale intensity I_{GS} normalized by the incident illumination intensity I_0 is shown as a function of square size s in figure 1(B). Thirty grayscales were chosen for ease of photomask design and economy. Many more grayscales can be rendered by varying the diffractive array lattice structure, pitch, or element shape, or by specifying a photomask with improved critical dimension tolerance and uniformity [26]. Non-planar nanofluidic structures with submicrometer lateral dimensions could also be fabricated by reducing the width of the diffractive arrays to one diffractive element per unit pitch [29].
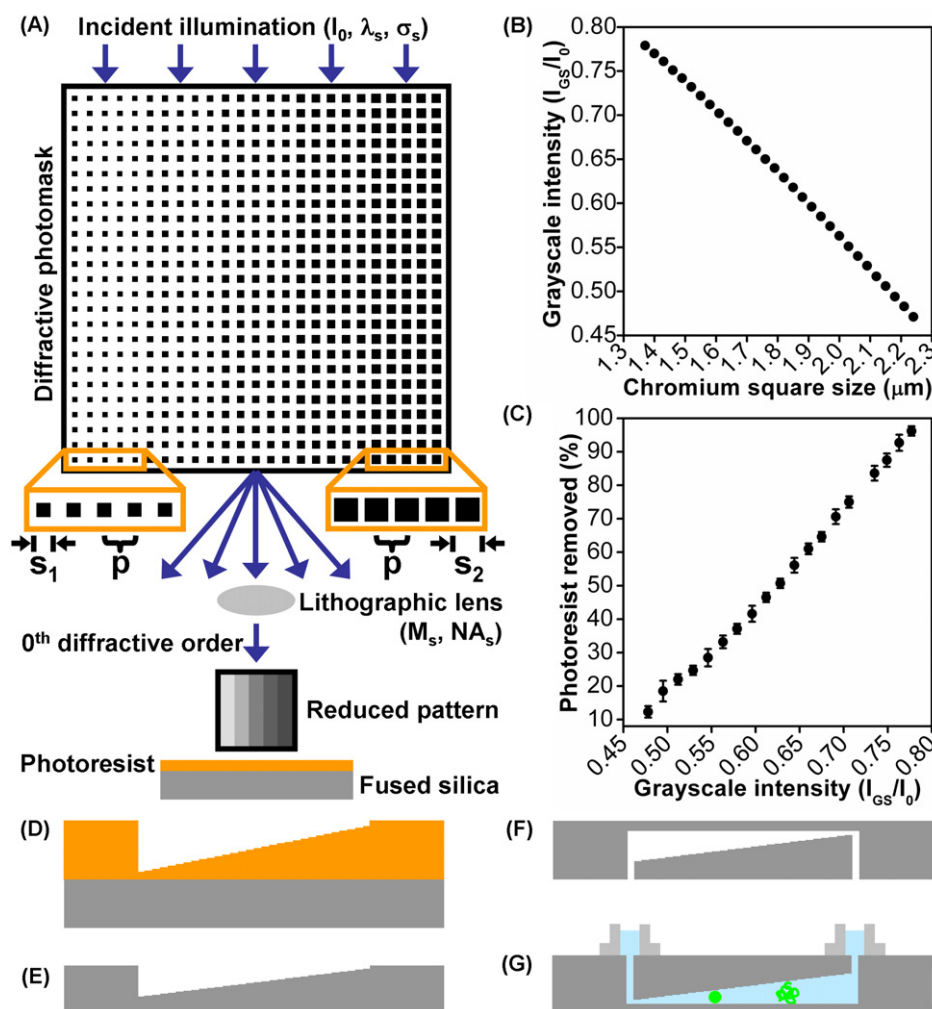
Figure 1. Nanofabrication process. (A) Schematic of a chromium-on-quartz photomask used with a reduction stepper as a diffraction filter to produce grayscales of variable intensity. (B) Grayscale intensity modeled as a function of diffractive square size s on a pitch p of 4 μm. (C) Photoresist response to grayscale exposure characterized with a calibration photomask. (D) Cross-sectional schematic of a 3D staircase function pattern generated in a thin film of photoresist. (E) Schematic of nanoscale pattern transfer into a fused silica substrate with reactive ion etching. (F) Schematic of fluidic access holes micro-abrasive blasted through the substrate wafer and formation of an enclosed 3D nanofluidic structure with glass wafer bonding. (G) Schematic of reservoirs attached to the substrate wafer to load solutions of nanoparticles and biomolecules into the device.

Fused silica substrate wafers with a thickness of 0.50 mm and a surface roughness of $\leqslant$0.5 nm, as specified by the manufacturer, were spin coated with a thin film of broadband positive tone photoresist with a thickness of (1069 $\pm$ 5) nm (mean $\pm$ standard deviation). The diffractive photomask was used with a reduction stepper of magnification $M_s = 0.2\times$, wavelength $\lambda_s = 436$ nm, partial coherence parameter $\sigma_s = 0.43$, and numerical aperture $NA_s = 0.3$ to render grayscales on a substrate for the top-down partial exposure of its photoresist etch mask, which was then fully developed. Prior to fabrication of the structures presented in this paper, a calibration photomask was used to characterize the response of the photoresist to grayscale exposure. The results of this calibration are shown in figure 1(C). The incident illumination intensity I_0 was the dose required to fully clear the photoresist during development. An approximately linear response occurred over a usefully large range, simplifying subsequent nanofabrication process design.

3D structure patterns in the photoresist etch mask were transferred to the fused silica substrate using a low selectivity CHF_3/O_2 reactive ion etch process, as illustrated in figures 1(D) and (E). For each grayscale, the corresponding region of the photoresist etch mask was completely etched away and the underlying fused silica substrate was subsequently etched for a particular duration in one continuous process. Different etch selectivities and durations were used to fabricate nanostructures with staircase function surface topographies and different depth profiles and depth offsets from a single photomask, as shown in figure 2(A). Two staircase structures were fabricated to demonstrate the extent of control over nanoscale pattern transfer. The less selective etch was used to make a 'shallow' staircase structure ($\blacksquare$) with steps of $\approx$11 nm in depth, no depth offset, and depths controlled from (11 $\pm$ 4) nm to (332 $\pm$ 4) nm (mean $\pm$ standard deviation) across the 120 μm structure width. The more selective etch was used to make a 'deep' staircase structure ($\bullet$)
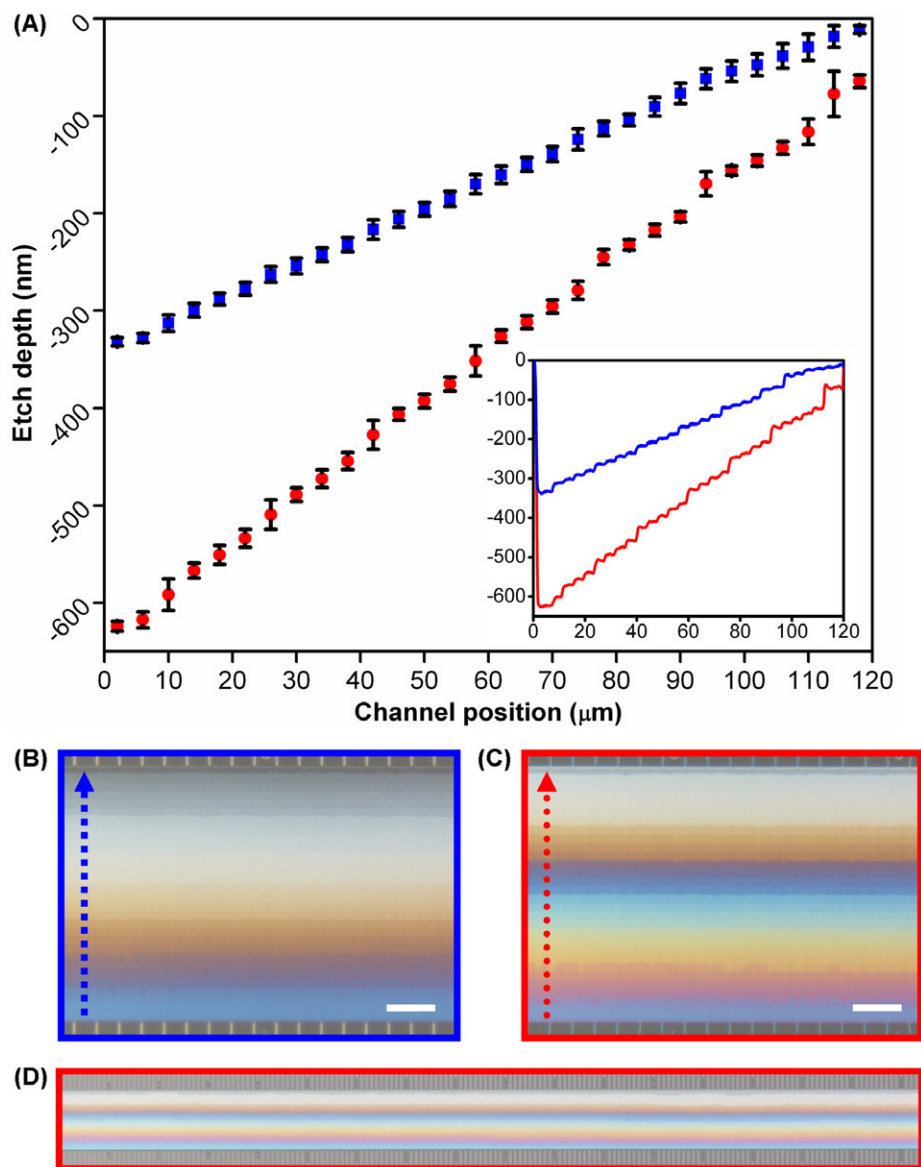
Figure 2. 3D nanofluidic structures. (A) Depth profiles of shallow and deep staircase structures controlled from (11 ± 4) nm to (332 ± 4) nm (■) and from (64 ± 4) nm to (624 ± 5) nm (●), (mean $\pm$ standard deviation). Error bars represent the standard deviation of 13 scanned probe measurements taken at 1 mm intervals along the structure lengths. Individual representative scans are shown in the inset. (B) Brightfield optical micrograph of an air-filled nanofluidic structure with depths ranging from ≈10 to ≈330 nm, top to bottom, corresponding to the shallow structure in (A). White light interference patterns show discrete changes in structure depth. (C) Brightfield optical micrograph of a nanofluidic structure with depths ranging from ≈60 to ≈620 nm, top to bottom, corresponding to the deep structure in (A). (D) Brightfield optical micrograph of a 1.7 mm length of the structure shown in (C). Scale bars are 20 μm.

with steps of ≈19 nm in depth, a depth offset of approximately two-and-a-half steps, and depths controlled from (64 ± 4) nm to (624 ± 5) nm (mean $\pm$ standard deviation) across the 120 μm structure width. These measurements were made with a scanned probe surface profilometer. Mean depth values were obtained from the central portion of each step not obscured by artifacts resulting from the micrometer scale probe tip scanning over step edges. Representative individual scans shown in the inset of figure 2(A). Error values represent the standard deviation of 13 scanned probe measurements separated by 1 mm along the entire 1.2 cm length of the structures. The average standard deviation of an etch depth was 8 nm for the

shallow structure (■) and 9 nm for the deep structure (●) in figure 2(A), with similar variation between devices fabricated across 100 mm wafers. The less selective and more selective etches resulted in root mean square surface roughness values of ≈3 nm (■) and ≈2 nm (●), respectively, as measured with an atomic force microscope equipped with an etched single crystal silicon probe operated in tapping mode. Periodic perturbations of the photoresist film thickness and etch depth profile occurred across both structure widths. A probable cause of these patterns is a thin film interference effect that occurred during grayscale photoresist exposure (data not shown), but a full characterization and elimination of this phenomenon is

left to future work. As illustrated in figure 1(F), inlet and outlet holes were micro-abrasive blasted through the substrate, which was cleaned and bonded to a fused silica cover wafer with a thickness of 0.17 mm and a surface roughness of ⩽0.5 nm, as specified by the manufacturer. The bonded wafer stack was annealed at ≈1100 °C. Subsequent scanned probe measurements of the outside of the cover wafer confirmed no outward deflection resulting from nanoglassblowing [18], which indicates that etch depths measured prior to wafer bonding accurately represent the resulting nanofluidic structure depths. Representative brightfield optical micrographs of air-filled 3D nanofluidic structures corresponding to the shallow and deep etch depth profiles in figure 2(A) are shown in figures 2(B) and (C), respectively. Distinct nanoscale structure depths are made evident by discrete color spectrums resulting from white light interference patterns [30]. The structure in figure 2(B) had depths controlled from ≈10 to ≈330 nm, from the top to the bottom of the image, and the structure in figure 2(C) had depths between ≈60 and ≈620 nm, with the same orientation. A brightfield optical micrograph of a 1.7 mm length of the structure in figure 2(C) is shown in figure 2(D), giving a millimeter range view of the channel.

4. Materials and methods

Reservoirs were attached to the substrate to introduce samples into the 3D structure, as illustrated in figure 1(G). Fluorescent polystyrene spheres with a diameter of 100 nm, as specified by the manufacturer, and absorption and emission peaks at 505 nm and 515 nm, respectively, were diluted in phosphate buffered saline solution. Bacteriophage λ DNA molecules with a length of 48.5 kilobase pairs, as specified by the manufacturer, were labeled for fluorescence microscopy with an intercalating dimeric cynanine nucleic acid dye with absorption and emission peaks at 491 nm and 509 nm, respectively, at a ratio of 5 base pairs per dye molecule and diluted in tris-acetate-ethylenediaminetetraacetic-acid 5X buffer with a volume fraction of ≈1% of 2-mercaptoethanol added to reduce photobleaching. Platinum wire electrodes were sealed inside of the sample reservoirs to provide electrical contact with the solution.

An inverted optical microscope was used in epifluorescence mode to image samples through the cover wafer with a plan apochromat oil immersion objective of magnification $M_o = 63\times$ and numerical aperture $NA_o = 1.4$. A metal halide arc lamp was used with a 450–490 nm band pass filter for fluorescence excitation. Fluorescence emission was isolated with a 495 nm dichroic mirror and refined with a 500–550 nm band pass filter. Videos and images were acquired with an electron multiplying charge coupled device camera.

5. Results and discussion

100 nm polystyrene spheres and bacteriophage λ DNA molecules were used to demonstrate the size exclusion of rigid nanoparticles and the variable confinement and deformation of large biopolymers, as illustrated in figure 3(A). A prototype 3D nanofluidic structure with depths varying from ≈50 to ≈550 nm in a staircase function profile across the structure width was utilized for these experiments. An electric field gradient was applied to this structure via arrays of submicrometer fluidic channels with widths of 1.0 μm and depths of ≈550 nm, as seen at the top and bottom of figures 2(B)–(D). These arrays were used to connect the deep and shallow edges of the 3D nanofluidic structure to wider channels with submicrometer depths leading to sample reservoirs, as illustrated in figure 3(B). Voltages were applied at V_i, and samples were injected into the deep side of the 3D nanofluidic structure at I.

Polystyrene nanoparticles were loaded into the structure and driven electrophoretically down its length and across its width towards the shallow side. A fluorescence micrograph of nanoparticles in the structure is shown in figure 3(C), with the shallow edge of the structure at the top of the image and the deep edge of the structure at the bottom. The top part of the structure remained free of nanoparticles, which were precluded from entering regions of the structure with depths less than the hydrodynamic diameter. This size exclusion mechanism suggests the future use of 3D nanofluidic devices for the spatial separation and metrology of mixtures of analytes with different nanoscale sizes and structural properties such as rigidity, such as distributions of nanoparticles or the contents of a single cell. The range and resolution of such manipulations and measurements would depend on control of device depths over the full span of analyte sizes, or within discrete ranges for a mixture of analytes with a multimodal size distribution. 3D nanofluidic devices would have a significant advantage in this regard over nanofluidic structures limited to several depths by conventional nanofabrication processes.

Bacteriophage λ DNA molecules at a low initial concentration of ≈1 μg ml⁻¹ were driven into the same structure with a low electric field of ≈2 V cm⁻¹ for single molecule analysis. While not excluded from any regions of the structure, ≈50 DNA molecules demonstrated complex dynamic behavior and assumed qualitatively different conformations as a function of structure depth and entropic confinement. When driven down the length and across the width of the structure, molecules made discrete transitions into shallower depths and would sometimes elongate from a coiled conformation. A representative fluorescence micrograph of several DNA molecules in the structure is shown in figure 3(D), with the same orientation as figure 3(C). Enlarged images of two molecules are shown in the inset. DNA molecules that were forced into shallow regions of the structure, as shown in figure 3(D) (i), generally became more elongated than molecules in deeper regions, as shown in figure 3(D) (ii), as expected [18]. A full account of this behavior is beyond the scope of this paper, but these results suggest the future use of 3D nanofluidic devices for the detailed investigation of nanoscale confinement effects on biopolymers. This rapidly growing field of research would benefit from 3D nanofluidic devices with numerous, precisely controlled depths to meticulously map parameter spaces with confinement regimes that have been predicted theoretically but not yet elucidated experimentally [31]. On-chip applications that exploit engineered variation in nanoscale entropic confinement
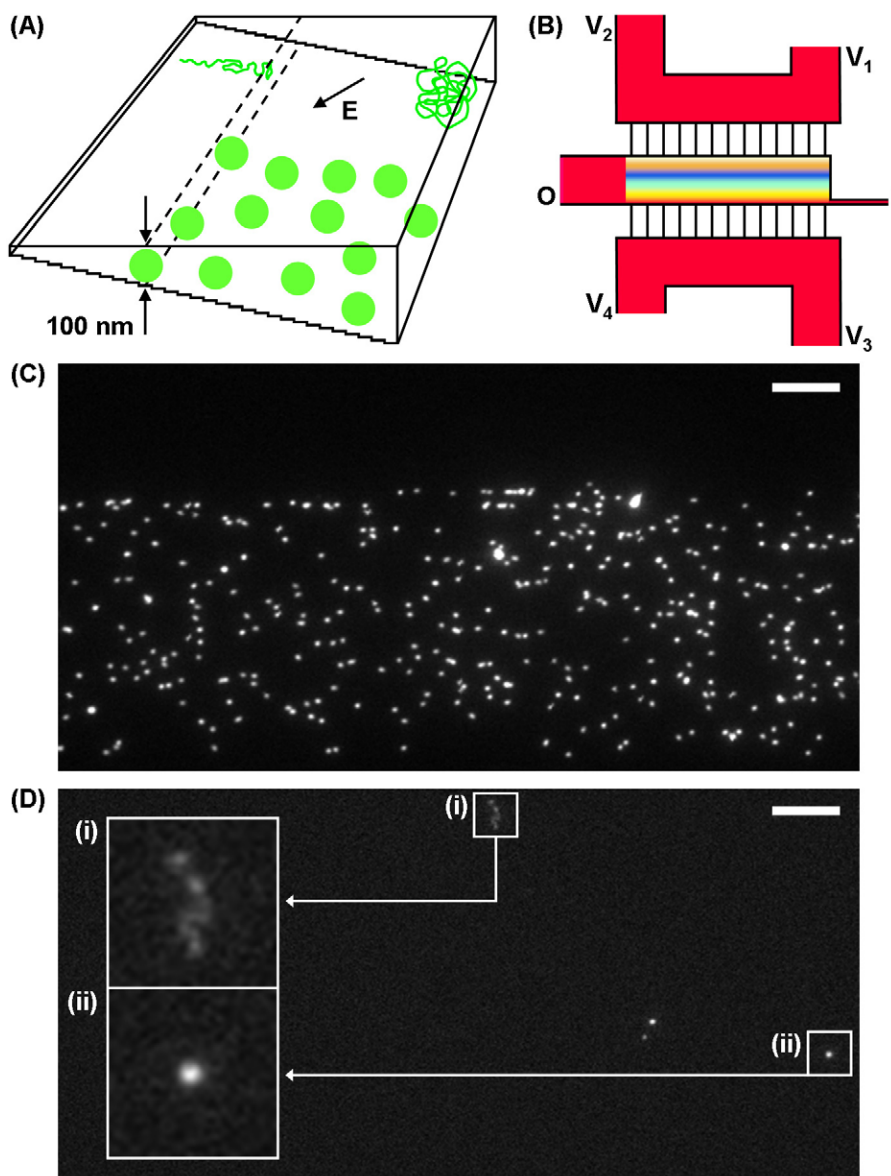
Figure 3. Nanoparticle and biomolecule manipulation. (A) Schematic of nanoparticle size exclusion and biomolecule confinement and deformation in a 3D nanofluidic structure with a staircase function surface topography. (B) Schematic of nanofluidic device design with inlet (I), outlet (O) and voltage application (V_i) channels. (C) Fluorescence micrograph of 100 nm polystyrene spheres in a 3D nanofluidic structure with a staircase function depth profile ranging from ≈50 nm at the top edge of the image to ≈550 nm at the bottom edge. Nanoparticles were excluded from regions of the staircase structure with depths less than the hydrodynamic diameter. (D) Fluorescence micrograph of bacteriophage λ DNA molecules in the same structure, which assumed qualitatively different conformations as a function of structure depth and confinement. Scale bars are 20 μm.

of biopolymers, such as the sieving of DNA mixtures [15] or the adiabatic funneling of long DNA molecules [17], could also benefit from nanofluidic devices with complex three-dimensional surface topographies.

6. Conclusion

Nanofluidic devices have unique advantages for the manipulation and analysis of nanoscale analytes, but almost all nanofluidic structures have remained limited in form and function by planar fabrication processes. This paper presents the first nanofluidic structures with complex three-dimensional surfaces of arbitrary design, fabricated with conventional in-tegrated circuit manufacturing tools and a single layer of grayscale photolithography. This accessible nanofabrication process will facilitate the future implementation and on-chip integration of 3D nanofluidic structures. A prototype 3D nanofluidic device was used to demonstrate the size exclusion of rigid nanoparticles and the variable confinement and deformation of biomolecules. These results show the potential of 3D nanofluidic structures to increase the range and resolution of nanofluidic analytical applications, such as the spatial separation and metrology of complicated mixtures of nanoscale analytes, and enable nanoscale and single molecule investigations in exceptional detail.

Acknowledgments

References

[1] Tegenfeldt J O, Prinz C, Cao H, Huang R L, Austin R H, Chou S Y, Cox E C and Sturm J C 2004 *Anal. Bioanal. Chem.* **378** 1678–92
[2] Mannion J T and Craighead H G 2007 *Biopolymers* **85** 131–43
[3] Reccius C H, Stavis S M, Mannion J T, Walker L P and Craighead H G 2008 *Biophys. J.* **95** 273–86
[4] Stavis S M, Corgie S C, Cipriany B R and Craighead H G 2007 *Biomicrofluidics* **1** 034105
[5] Liang X G and Chou S Y 2008 *Nano Lett.* **8** 1472–6
[6] Li J, Stein D, McMullan C, Branton D, Aziz M J and Golovchenko J A 2001 *Nature* **412** 166–9
[7] Tegenfeldt J O *et al* 2004 *Proc. Natl Acad. Sci. USA* **101** 10979–83
[8] Foquet M, Korlach J, Zipfel W R, Webb W W and Craighead H G 2004 *Anal. Chem.* **76** 1618–26
[9] Hsieh C C, Balducci A and Doyle P S 2008 *Nano Lett.* **8** 1683–8
[10] Hsieh C C, Balducci A and Doyle P S 2007 *Macromolecules* **40** 5196–205
[11] Strychalski E A, Levy S L and Craighead H G 2008 *Macromolecules* **41** 7716–21
[12] Cross J D, Strychalski E A and Craighead H G 2007 *J. Appl. Phys.* **102** 024701
[13] Jo K, Dhingra D M, Odijk T, de Pablo J J, Graham M D, Runnheim R, Forrest D and Schwartz D C 2007 *Proc. Natl Acad. Sci. USA* **104** 2673–8
[14] Han J and Craighead H G 2000 *Science* **288** 1026–9
[15] Fu J P, Schoch R B, Stevens A L, Tannenbaum S R and Han J Y 2007 *Nat. Nanotechnol.* **2** 121–8
[16] Xia Y N, Rogers J A, Paul K E and Whitesides G M 1999 *Chem. Rev.* **99** 1823–48
[17] Cao H, Tegenfeldt J O, Austin R H and Chou S Y 2002 *Appl. Phys. Lett.* **81** 3058–60
[18] Strychalski E A, Stavis S and Craighead H G 2008 *Nanotechnology* **19** 315301
[19] Li B, Yu H, Sharon A and Zhang X 2004 *Appl. Phys. Lett.* **85** 2426–8
[20] Ke K, Hasselbrink E F and Hunt A J 2005 *Anal. Chem.* **77** 5083–8
[21] Andersson H, Ekberg M, Hard S, Jacobsson S, Larsson M and Nilsson T 1990 *Appl. Opt.* **29** 4259–67
[22] Geissler M and Xia Y N 2004 *Adv. Mater.* **16** 1249–69
[23] Oppliger Y, Sixt P, Stauffer J M, Mayor J M, Regnault P and Voirin G 1994 *Microelectron. Eng.* **23** 449–54
[24] Waits C M, Morgan B, Kastantin M and Ghodssi R 2005 *Sensors Actuators* a **119** 245–53
[25] Atencia J, Barnes S, Douglas J, Meacham M and Locascio L E 2007 *Lab Chip* **7** 1567–73
[26] Henke W, Hoppe W, Quenzer H J, Staudtfischbach P and Wagner B 1994 *Japan. J. Appl. Phys.* 1 **33** 6809–15
[27] Goodman J W 2004 *Introduction to Fourier Optics* 3rd edn (New York: McGraw-Hill)
[28] *Microlithography: Science and Technology* 2007 2nd edn (Boca Raton, FL: CRC Press)
[29] Waits C M, Modafe A and Ghodssi R 2003 *J. Micromech. Microeng.* **13** 170–7
[30] Lin C and Sullivan R F 1972 *J. Res. Dev.* **16** 269
[31] Odijk T 2008 *Phys. Rev.* E **77** 4